

1 Unusual neon isotopic composition in Neoproterozoic sedimentary rocks: fluorine bearing
2 mineral contribution or trace of an impact event?

3
4 Déborah Chavrit¹, Manuel A. Moreira^{1*}, David A. Fike², Frédéric Moynier^{1,3}

5
6 ¹ Institut de Physique du Globe de Paris, Sorbonne Paris Cité, Univ Paris Diderot, CNRS, F-
7 75005 Paris, France

8 ² Department of Earth and Planetary Sciences, Washington University, St Louis, Missouri 63130,
9 USA

10 ³ Institut Universitaire de France, Paris, France

11
12 * corresponding author

13
14 **Contacts:**

15 Déborah Chavrit: deborahchavrit@gmail.com

16 Manuel A. Moreira: Moreira@ipgp.fr

17 David A. Fike: dfike@levee.wustl.edu

18 Frédéric Moynier: Moynier@ipgp.fr

19
20 **Keywords**

21 noble gas; Ediacaran sedimentary rocks; Ne-A; nucleogenic; fluorite; Acraman impact

22
23 **Highlights**

- 24
- 25 • Helium and neon isotopes have been measured in Huqf supergroup in Oman
 - 26 • Neon shows a peculiar isotopic signature suggesting either a major extraterrestrial impact
27 or a peculiar enrichment in fluorine
- 28
29

30 **Abstract**

31 Extraterrestrial materials have He and Ne isotopic compositions that are distinct from those of
32 the Earth's surface. In order to track the extraterrestrial material accreted onto Earth during the
33 Ediacaran period, we have analyzed the He and Ne isotopic composition of thirteen sedimentary
34 rocks in the age range ~550-600 Ma, coming from the Huqf supergroup in Oman for which
35 carbon and sulfur isotopic data have been characterized previously.

36 $^3\text{He}/^4\text{He}$ ratios range between 0.006 ± 0.003 and $0.27\pm 0.01 R_A$, with R_A being the atmospheric
37 ratio. $^3\text{He}/^4\text{He}$ ratios show a positive relationship with ^3He contents ranging between 0.6 and 31
38 $\times 10^{-13} \text{ cm}^3 \text{ STP.g}^{-1}$. The ^3He contents are within the literature data for 3 to 480 Myr old samples
39 with evidence of IDP ^3He (IDP for interplanetary dust particles), suggesting that extraterrestrial
40 ^3He is still retained in such old samples.

41 $^{20}\text{Ne}/^{22}\text{Ne}$ ratios are close to or below the modern atmospheric ratio of 9.8 with the minimum
42 value equal to 9.05 ± 0.03 . $^{21}\text{Ne}/^{22}\text{Ne}$ ratios show a high range of variation, going from
43 0.0345 ± 0.0009 to 0.0935 ± 0.0023 . The Ne isotopic compositions follow a nucleogenic trend
44 similar to that of crustal fluids from the literature and predicted continental crust. However, one
45 sample (3404) shows an unusual Ne isotopic composition with a lower $^{20}\text{Ne}/^{22}\text{Ne}$ at similar
46 $^{21}\text{Ne}/^{22}\text{Ne}$ compared to the other samples.

47 Two hypotheses can explain this singular Ne isotopic composition. First, it could be the result of
48 a particular nucleogenic trend due to the presence of F-bearing minerals in this sample. SEM-
49 EDS elemental mapping showed that although F- and Ca-rich phases, which could correspond to
50 fluorites, are present in sample 3404. However, their abundance of ~0.15% seem too low to
51 explain the unusual Ne isotopic composition. However, due to the high uncertainty of the
52 calculations, we cannot totally rule out this hypothesis. Alternatively, the singular Ne isotopic
53 composition could be due to the presence of a Ne-A component, a component characterizing pre-
54 solar diamonds contained in chondrites. This would indicate that a major object impacted the
55 Earth at the time the sediment was forming, between ~600 and ~550 Ma, which is coherent with
56 the estimated age range of the Acraman impact in Australia.

57

58

59

60 **1 Introduction**

61

62 The accretion of extraterrestrial material falling onto Earth can be tracked using geochemical
63 tracers, which are more abundant and isotopically distinct in the extraterrestrial materials
64 compared to the Earth's surface. For example, Ir concentrations, He isotopes and Os isotopes
65 (e.g. (Peucker-Ehrenbrink 2001)) and Cr isotopes (Mougel et al., 2017) are particularly well
66 suited geochemical tracers. Amongst those elements, He has the largest abundance variations
67 between extraterrestrial and terrestrial material, with ^3He abundances and $^3\text{He}/^4\text{He}$ ratios in
68 extraterrestrial material respectively $\sim 10^9$ and $\sim 10^5$ times higher than that of the Earth's crustal
69 rocks (see review in (McGee and Mukhopadhyay, 2013)). Consequently, the measurements of
70 He isotopes in marine sediments, or sedimentary rocks of different ages have been the subject of
71 numerous studies for several decades, in order to track the accretion of extraterrestrial material
72 onto Earth over geological timescales (e.g. (Amari and Ozima, 1988; Farley et al., 2006;
73 Marcantonio et al., 1995; Murphy et al., 2010; Takayanagi and Ozima, 1987))

74 However, since He is an element with a high diffusivity (Hiyagon, 1994), it is likely to be
75 partially or totally lost from the samples either during their entry into the atmosphere or after
76 their deposition at the Earth's surface. For instance, among the extraterrestrial micrometeorites
77 falling onto Earth, He can only be retained in the smallest ones (e.g. $< 10\mu\text{m}$) because, due to
78 their micrometric size, they experience less frictional heating during their entry in the Earth
79 atmosphere than bigger objects (Farley et al., 1997).

80 Although the oldest samples with a record of extraterrestrial ^3He are 480 Ma old carbonates
81 (Patterson et al., 1998), due to its high diffusivity, He is likely to be partially or totally lost
82 during its stay at the surface for millions of years. Thus, it is interesting to focus on Ne isotopes,
83 because Ne is less sensitive to diffusion than He. According to the diffusion experiments of
84 (Hiyagon, 1994), Ne would be retained in IDP at typical seafloor temperatures during the transit
85 times of the ocean crust on the seafloor, unlike He, which would be significantly released from
86 the IDP at these temperatures over million-year timescales.

87 Moreover, Ne isotopes have also distinct signatures in extraterrestrial materials compared to the
88 Earth's surface. The Ne IDP signature is close to that of the Ne-B value (12.52 ± 0.18 , (Black,

89 1972), 12.73 ± 0.02 , (Moreira, 2013; Moreira and Charnoz, 2016) and has been recently recorded
90 in marine sediments together with IDP-derived He (Chavrit et al., 2016). Ne-B results from
91 irradiation and sputtering processes in space (Moreira, 2013). As such, it preferentially is found
92 in the outer 100 nm of objects and thus recovered in objects with a high surface to volume ratio
93 such as IDP. Bigger objects such as meteorites can also include the Ne-B component if they
94 derive from a regolith, however, they can additionally contain the Ne-A component (e.g. (Black,
95 1972; Pepin, 1967)), which has been recorded in pre-solar nano-diamonds (Huss and Lewis,
96 1994) and is particularly found in carbonaceous chondrites (see review in (Moreira, 2013)).
97 Those two extraterrestrial signatures are distinct from the one that characterizes the material at
98 the surface of the Earth. Combining He and Ne isotopes can allow to assess the amount of He
99 lost from the samples (Chavrit et al., 2016). Thus, this could be used to trace the accretion of
100 different size ranges of the extraterrestrial material falling onto Earth. Neon being less sensitive
101 to diffusion than He, it has the potential to trace different size ranges of extraterrestrial objects
102 accreting onto Earth (from micrometeorites to meteorites).

103

104 In this study, we coupled He and Ne isotopic measurements in samples of ~550 to ~600 Ma old
105 sedimentary rocks from the same location in Oman in order to trace the extraterrestrial material
106 accretion during this time period.

107

108 **2 Samples and geological context**

109

110 The samples are 13 limestones, dolostones and calcareous shale from the Ediacaran-aged Huqf
111 Supergroup in Oman. Samples come from MQR-1 well and span a depth range from 3228 –
112 3936 m, corresponding to the Khufai, Shuram, and Buah formations of the Nafun group. The
113 samples are believed to have been deposited in the interval between ~600 Ma to ~550 Ma
114 (Figure 1) (Bowring et al., 2003; Condon et al., 2005; Fike et al., 2006; Grotzinger et al., 1995;
115 Le Guerroué et al., 2006), although the middle Ediacaran interval has notoriously poor
116 chronostratigraphic resolution, frustrating attempts to link together records of environmental and
117 ecological change over this critical interval of Earth history.

118 These samples have been previously characterized for their carbon and sulfur isotopic
119 composition (Burns and Matter, 1993; Fike et al., 2006). The data record the largest known

120 $\delta^{13}\text{C}_{\text{carbonate}}$ negative excursion in Earth history, called the Shuram excursion, which is
121 characterized by $\delta^{13}\text{C}_{\text{carb}}$ values decreasing to -12‰ (Fike et al., 2006), Figure 1).
122 The origin of this excursion is still subject to debate. The Shuram excursion was first attributed
123 to diagenetic alteration (Burns and Matter, 1993). However, methods to assess the diagenesis
124 process have failed to validate this hypothesis (Le Guerroué, 2010). In addition, this excursion
125 has been documented in multiple sites in the world, and it is more likely that the $\delta^{13}\text{C}_{\text{carbonate}}$
126 values reflect a primary signal encoded into the sediments during deposition (Fike et al., 2006;
127 Grotzinger et al., 2011 ; Le Guerroué and Cozzi, 2010).

128

129

130 **3 Methods**

131

132 **3.1 He and Ne isotopes measurements**

133

134 The sediment sample preparation is the same as in (Chavrit et al., 2016). Fractions of powdered
135 samples weighting between 0.2 and 2 g (Table 1) were decarbonated on a heating plate at 60°C
136 using 10% acetic acid. For noble gas analysis, the carbonate fraction of the samples has to be
137 removed to improve the gas purification. After three rinsing with milliQ water, each residue was
138 dried at 60°C and packed into 1 or 2 Al foil packets, allowing for the measurement of duplicates.
139 Sample 3404 was prepared twice. The packets were loaded into a sample tree made of Pyrex
140 connected to the mass spectrometer. The extraction line was baked out at ~120°C and sample
141 tree baked out at ~60°C for ~12 h during pumping prior to the measurements. The gases were
142 extracted from the samples under high vacuum using a furnace at 1200°C. After purification, the
143 ^3He , ^4He , ^{20}Ne , ^{21}Ne and ^{22}Ne were sequentially analyzed using the Noblesse mass spectrometer
144 (Nu instruments) located at the Institut de Physique du Globe de Paris (IPGP), France, following
145 the method described in (Chavrit et al., 2016). Together with an air standard for Ne, the isotopic
146 compositions of the homemade gas standard used to calibrate the data are the following:
147 $^3\text{He}/^4\text{He}=7.73 \text{ R}_A$, $^{20}\text{Ne}/^{22}\text{Ne}=9.94$, $^{21}\text{Ne}/^{22}\text{Ne}=0.0309$. On average, the furnace blank values,
148 made at a temperature of 1200°C, were $6\times 10^{-9} \text{ cm}^3 \text{ STP}$ for ^4He and $3.6\times 10^{-12} \text{ cm}^3 \text{ STP}$ for ^{22}Ne .
149 Seven duplicates were analyzed in order to assess the reproducibility of the measurements.
150 Duplicates of each sample were all from the same residual fraction which was split into several

151 Al foil packets, except for sample 3404 which aliquots 2 and 3 were from a residual fraction
152 different from that of aliquot 1 (Table 1).

153 In order to understand the origin of the Ne composition of the samples, we publish data of 3
154 Durango fluorapatites (Table 1) analyzed in 2006 by laser heating (Yb doped fiber laser) using
155 the ARESIBO mass spectrometer at the IPGP (Moreira and Allègre, 2002).

156

157

158 **4 Results**

159

160 The results are reported in Table 1. The non-carbonate fractions (NCF) range from 11% for the
161 dolostone at 3428 m depth to 73% for the calcareous shale at 3722 m depth. $^3\text{He}/^4\text{He}$ ratios range
162 between $0.006 \pm 0.003 R_A$ (3228#1) and $0.27 \pm 0.01 R_A$ (3404#2). R_A is the atmospheric ratio, with
163 a value of 1.384×10^{-6} (Clarke et al., 1976b). The three highest $^3\text{He}/^4\text{He}$ ratios are similar and
164 correspond to the 3 duplicates of 3404, indicating a good reproducibility of the results. ^3He
165 contents range between 0.6 and $31 \times 10^{-13} \text{ cm}^3 \text{ STP.g}^{-1}$. They are in the same range as the data
166 from the literature on samples that show evidence for an extraterrestrial ^3He contribution (Figure
167 2). In addition, our He data show a positive correlation between the ^3He content and the $^3\text{He}/^4\text{He}$
168 ratio, confirming the mixing of an extraterrestrial IDP component and a terrestrial component in
169 the samples. $^3\text{He}/^4\text{He}$ positively correlates with ^4He and ^3He meaning that these two isotopes
170 contribute to the variation of the ratio, which can be related both to the contribution of radiogenic
171 ^4He from the terrestrial component and to the contribution of ^3He from the extraterrestrial
172 component.

173

174 $^{20}\text{Ne}/^{22}\text{Ne}$ ratios are close to or below the atmospheric ratio of 9.8 (Eberhardt et al., 1965), with
175 the minimum values equal to 9.05 ± 0.03 for sample 3636 (Figure 3). $^{21}\text{Ne}/^{22}\text{Ne}$ ratios show a high
176 range of variation, going from 0.0345 ± 0.0009 (3360#1) to up to three times the atmospheric ratio
177 of 0.0290 (Eberhardt et al., 1965) with the data of sample 3636 ($^{21}\text{Ne}/^{22}\text{Ne} = 0.0935 \pm 0.0023$).

178 In Figure 1, different trends are highlighted in the evolution of the NCF and the noble gases
179 isotopic ratios over time and depth. From 3936 m to 3722 m, the NCF progressively increases
180 from 16% to reach a maximum value of 73%. Then, the NCF follows a constant decrease down
181 to 11% at 3428 m, followed by a relatively regular increase up to 30% at 3228 m. $^3\text{He}/^4\text{He}$ ratios

182 do not show a clear evolution, apart from two sharp positive peaks at 3826 m and 3404 m.
183 $^{20}\text{Ne}/^{22}\text{Ne}$ ratios and $^{21}\text{Ne}/^{22}\text{Ne}$ ratios show an opposite evolution. Whereas $^{20}\text{Ne}/^{22}\text{Ne}$ ratios
184 decrease progressively from 3936 m to reach a minimum value at 3636 m, the $^{21}\text{Ne}/^{22}\text{Ne}$ ratios
185 increase. Between 3636 m and 3428 m, the $^{20}\text{Ne}/^{22}\text{Ne}$ ratios increases whereas the $^{21}\text{Ne}/^{22}\text{Ne}$
186 ratio decreases. At 3404 m, the $^{20}\text{Ne}/^{22}\text{Ne}$ ratios show a sharp negative spike, associated to a
187 positive $^3\text{He}/^4\text{He}$ peak. Three duplicates of the sample at 3404 m show the same composition
188 (Table 1) excluding a possible analytical problem during the measurement.

189

190 **5 Discussion**

191

192 In this part, we will highlight an unusual Ne isotopic signature. We will detail the two
193 hypotheses that could explain such value.

194

195 **5.1 The recording of an unusual Ne signature**

196

197 In a $^{20}\text{Ne}/^{22}\text{Ne}$ vs $^{21}\text{Ne}/^{22}\text{Ne}$ diagram, our new data do not plot in the same area as previously
198 analyzed terrestrial sediments (Figure 3), that showed evidence of IDP derived Ne (Chavrit et al.,
199 2016). It does not necessarily mean that IDP are absent from the samples. More preferentially,
200 the Ne IDP signal may be overprinted, as it is also the case for helium, because the samples
201 contain much higher NCF than the samples of (Chavrit et al., 2016) (Annex Figure A1 of the
202 supplementary material).

203 Except for the sample at 3404 m, our samples fall into the field defined by crustal fluids (Holland
204 et al., 2013; Kennedy et al., 1990; Lippmann-Pipke et al., 2011) or by the continental crust from
205 the KTB drill in Germany (Drescher et al., 1998). Sample 3404 presents an unusual Ne isotopic
206 composition, with a $^{20}\text{Ne}/^{22}\text{Ne}$ ratio lower than that of the other samples at similar $^{21}\text{Ne}/^{22}\text{Ne}$
207 ratio and falls outside this crustal fluid field. The three analyses of the Ne isotopic composition
208 of this sample are in excellent agreement (Table 1, Figure 3) indicating that this signature is not
209 an analytical artifact. In order to better understand this Ne isotopic composition, we have
210 calculated the slope of the mixing line going through each sample and the air component in the
211 Ne three isotopes diagram. In Figure 4, these slopes do not show a progressive evolution with
212 depth of the samples while the 3404m sample shows a strong negative spike. Consequently, this

213 unusual Ne isotopic signature seems to be localized and to only affect the layer at 3404 m. It
214 corresponds to the late stage of the Shuram excursion, at a slope break where the $\delta^{13}\text{C}$ starts to
215 recover more rapidly, at the beginning of the Buah formation (Figure 1). In the following we are
216 going to explore the two hypotheses that could explain such composition.

217

218 **5.2 A F-bearing mineral for the unusual Ne signature?**

219 **5.2.1 Neon nucleogenic production in Earth samples**

220

221 In the continental crust, the radioactive decay of $^{235,238}\text{U}$ and ^{232}Th produce α particles, most of
222 which stabilize in radiogenic ^4He . The other α particles react with surroundings atomic nuclei,
223 such as ^{17}O , ^{18}O and ^{19}F isotopes to produce respectively nucleogenic ^{20}Ne , ^{21}Ne and ^{22}Ne
224 (Figure 5). ^{20}Ne , ^{21}Ne and ^{22}Ne are also produced by neutron activation from ^{23}Na , ^{24}Mg , ^{25}Mg
225 (Figure 5), however, these reactions account for less than 1% of the Ne production in the crust
226 (Yatsevich and Honda, 1997). Based on the previous works of (Yatsevich and Honda, 1997) and
227 (Hünemohr, 1989), production rates (in $\text{cm}^3 \text{ STP g}^{-1} \cdot \text{yr}^{-1}$) have been empirically quantified by
228 (Ballentine and Burnard, 2002) as a function of the U, Th and F contents (in ppm) and O, Mg,
229 Na contents (in wt%), with the following equations:

230

$$231 \quad ^{20}\text{Ne produced} = (6.39[U] + 0.770[\text{Th}])(0.0226[\text{O}] + 0.0022[\text{Na}]) \times 10^{-22} \quad (1)$$

$$232 \quad ^{21}\text{Ne produced} = \{(1.48[U] + 0.186[\text{Th}])[\text{O}] + (0.105[U] + 0.0179[\text{Th}])[\text{Mg}]\} \times 10^{-22} \quad (2)$$

$$233 \quad ^{22}\text{Ne produced} = \{(3.06[U] + 0.417[\text{Th}])[\text{F}] + (4.20[U] + 0.663[\text{Th}])[\text{Mg}]\} \times 10^{-24} \quad (3)$$

234

235 These equations show that the nucleogenic $^{20}\text{Ne}/^{22}\text{Ne}$ and $^{21}\text{Ne}/^{22}\text{Ne}$ production ratios are
236 principally dependent on the O/F ratios of the samples as F is involved only on the production of
237 ^{22}Ne . As Mg is a major element, its natural variations of concentration remain small compared to
238 other trace elements such as F, U, Th. Variable O/F ratios will have the effect to change the
239 slopes of the mixing lines between the atmospheric endmember and the nucleogenic endmember
240 in a graph $^{20}\text{Ne}/^{22}\text{Ne}$ versus $^{21}\text{Ne}/^{22}\text{Ne}$ (Figure 3).

241 The continental crust nucleogenic trend predicted by (Yatsevich and Honda, 1997) corresponds
242 to a O/F ratio of 752 (atomic ratio) (Ballentine and Burnard, 2002), according to the previous

243 equations (1), (2) and (3). Archean fluids also follow a similar trend (Holland et al., 2013).
244 Crustal fluids data of (Kennedy et al., 1990) lie on a trend with O/F=113 (Ballentine and
245 Burnard, 2002). Almost all data from the literature, being crustal fluids of different ages, plot in
246 the field with an O/F ratio ranging from ~113 to ~752 (Figure 3).

247 After equations (1), (2) and (3), O/F ratios lower than 113 can be obtained for minerals very rich
248 in F and/or very poor in oxygen. It is the case for a full range of accessory minerals, for example
249 bastnäsite, containing 7.35 wt%F (O/F=4), or fergusonite (F=1.42 wt%, O/F=34) (Ballentine and
250 Burnard, 2002; Eikenberg et al., 1993; Hünemohr, 1989). It has the consequence of significantly
251 shifting common nucleogenic trends towards trends with more negative slopes (Figure 3). Some
252 major minerals can also present a low O/F ratio. For example, fluorite (CaF₂), which does not
253 contain any oxygen, is characterized by an O/F ratio of 0. Fluorapatite, the most common
254 phosphate mineral in the environment is also characterized by a low O/F (O/F=12). Neon
255 isotopic measurements of the Durango fluorapatite (Table 1, Figure 3) are in agreement with the
256 nucleogenic trend defined using O/F=12, determined theoretically using the mineral formula
257 (Ca₅(PO₄)₃F), suggesting that the empirical equations are reliable to estimate the ²⁰Ne/²²Ne and
258 ²¹Ne/²²Ne production ratios and consequently the nucleogenic trends.

259

260 **5.2.2 Unusual Ne signature: a particular terrestrial nucleogenic trend?**

261

262 Except one sample, our sedimentary rock samples fall into the same field as the one of crustal
263 fluids, corresponding to an O/F ratio ranging from ~113 to ~752 (Figure 3). For these samples,
264 the extents of the ²¹Ne/²²Ne ratios and ²²Ne contents are related to the non-carbonate fraction
265 (Annex Figure A1 of the supplementary material), an expected correlation since Ne is produced
266 by nuclear reactions of isotopes present in the detrital fraction of the samples, containing U and
267 Th.

268 On the other hand, an O/F equal to ~34 is required to explain the composition of the 3404 m
269 deep sample (Figure 3). An O/F ratio of 34 corresponds to the fergusonite (O=40.4 wt%, F=1.42
270 wt%), an accessory mineral phase. However, this sample could not only be composed of this
271 mineral, since it contains 85% carbonates (Table 1). Alternatively, it would be more probable
272 that the singular Ne isotopic composition could be the result of a mixing between an endmember

273 with production ratios similar to the one fitting the literature data and all the samples from this
274 study except at 3404 m, that is with $113 \leq O/F \leq 752$ and another endmember characterized by a
275 mineral phase with a O/F lower than 34 such as fluorapatite or fluorite characterized respectively
276 by $O/F=12$ and $O/F=0$ (Figure 3). The Ne isotopic compositions of these two endmembers can
277 be apprehended. The predicted crust production ratios are the following: $^{20}\text{Ne}/^{22}\text{Ne}=0.36$,
278 $^{21}\text{Ne}/^{22}\text{Ne}=3.67$ (Yatsevich and Honda, 1997), corresponding to an O/F ratio of 752 (Figure 3).
279 For the other endmember, we use the isotopic neon production ratios of fluorapatite
280 ($^{20}\text{Ne}/^{22}\text{Ne}=0.0043$; $^{21}\text{Ne}/^{22}\text{Ne}=0.0458$) and fluorite ($^{20}\text{Ne}/^{22}\text{Ne}=0$; $^{21}\text{Ne}/^{22}\text{Ne}=0$) that we
281 calculated using the elemental proportion calculated after their mineral formulae and equations
282 (1), (2) and (3). The details of our calculations are provided in the Annex 2 of the supplementary
283 material. After our calculations, the decrease of the O/F ratio from 752 down to 34 in order to fit
284 the data points of sample 3404 would require the presence of 96% ^{22}Ne derived from fluorite or
285 98% ^{22}Ne derived from fluorapatite in the sample.

286 Using equations (1), (2) and (3), we estimate that for 600 Ma old fluorites and fluorapatites, the
287 produced ^{22}Ne concentration is ~ 2 orders of magnitude higher than the ^{22}Ne concentration of the
288 samples from this study. It implies that ~ 0.4 to 37% fluorite, depending on the U and Th content
289 of the fluorine-bearing phase, would be sufficient to account for the Ne composition of the ~ 600
290 Ma old sample 3404. If the signal came exclusively from fluorapatite, this mineral would need to
291 have an abundance of 0.3-16%. To evaluate the presence of F in several of the samples, we
292 performed SEM-EDS elemental mapping for some of the residual fractions of the samples (non-
293 carbonate fractions) including sample 3404 (See Annex 3 of the supplementary material for the
294 details on the SEM measurements). The maps show some spots with a F-enrichment (Figure 6).
295 It is not possible to get reliable quantification of the data because the samples were powders that
296 were consequently not flat and Au-coated. Nevertheless, the decarbonated fraction of sample
297 3404 is the one which seems to visually contain the most abundant F-bearing phases amongst the
298 5 analyzed samples (Figure 6), particularly compared to sample 3428 which has a similar amount
299 of non-carbonate fraction. From these observations, it is thus possible that sample 3404 has an
300 O/F ratio lower than those of the other samples. However, a precise quantification is required to
301 determine if its O/F ratio is low enough to explain its peculiar Ne composition. This can be
302 assessed using theoretical calculations. The F-rich spots in sample 3404 are associated with Ca-
303 enrichments (Figure 6, Annex Figure A2 of the supplementary material), suggesting that these

304 phases are fluorites. We did not see any P peak associated with F peak in the spectra that could
305 witness the presence of fluorapatite. If we assume that all the F-rich phases in sample 3404 were
306 fluorite, we can estimate that ~1 wt.% of fluorite is present in the ~15 wt.% of the non-
307 carbonate fraction of sample 3404 (Table 1) analyzed with SEM-EDS (Figure 6), thus
308 corresponding to 0.15 wt.% of fluorite in the whole-rock sample. This first order calculation
309 gives a value too low to explain the composition of sample 3404. However, our calculations and
310 SEM measurements are not precise enough to be definite, especially because fluorite can contain
311 highly variable amounts of U and Th and that we did not consider any ejection factor of α
312 particles, which is dependent on the crystal size (Gautheron et al., 2006). Measurements of
313 fluorite crystals of different ages and sizes are needed to better evaluate the nucleogenic Ne
314 production in this mineral, in order to definitely test whether fluorite is responsible for the
315 peculiar Ne composition of sample 3404.

316

317 **5.3 A meteoritic origin for the unusual Ne signature?**

318

319 **5.3.1 The Ne-A component in sedimentary rocks**

320

321 In this study, the layer at 3404 m is characterized by an unusual Ne isotopic signature, with
322 $^{20}\text{Ne}/^{22}\text{Ne}=9.13-9.25$ and $^{21}\text{Ne}/^{22}\text{Ne}=0.0368-0.0373$ (Table 1). If this composition cannot be
323 explained by a nucleogenic trend (see previous section, 5.2), alternatively, it could be the result
324 of mixing three distinct components: air, “common” nucleogenic Ne and Ne-A (Figure 3). The
325 Ne-A component is a component present in meteorites, mainly in carbonaceous chondrites (see
326 review in (Moreira, 2013), with a distinct signature ($^{20}\text{Ne}/^{22}\text{Ne}=8.500\pm 0.057$,
327 $^{21}\text{Ne}/^{22}\text{Ne}=0.036\pm 0.001$, (Huss and Lewis, 1994) compared to those of the Earth’s surface, such
328 as air and crustal fluids (Figure 3). Consequently, a $^{20}\text{Ne}/^{22}\text{Ne}$ ratio below the air value and a
329 relatively low $^{21}\text{Ne}/^{22}\text{Ne}$ ratio in a sedimentary rock, such as in sample 3404, open the question
330 of the presence of a meteorite component in this sample. Such a component would imply that an
331 impact occurred on Earth at the time the sediment formed and that pre-solar nano-diamonds
332 contained in the bolide survived the impact, allowing this volatile element and thus the Ne-A
333 component to be trapped in the sediments. Darrah et al. measured a Ne isotopic composition in a

334 65 Ma old sediment from the LL-44 GPC-3 deep sea sediment core, with $^{20}\text{Ne}/^{22}\text{Ne}=8.85$ and
 335 $^{21}\text{Ne}/^{22}\text{Ne}=0.025$ ($n=2$), values very different from those characterizing their other samples
 336 (Darrah and Poreda, 2012). This composition is close to the Ne-A value. As evidenced from
 337 platinum group elements excesses and the presence of the large Chicxulub crater, the Earth
 338 underwent a large meteorite impact 65 Ma ago (e.g. (Alvarez et al., 1980; Hildebrand et al.,
 339 1991; Sharpton et al., 1992). Therefore, the presence of a Ne-A component in the sediments may
 340 be a witness of a major meteoritic impact. This peculiar neon isotopic signature is also associated
 341 to the highest $^3\text{He}/^4\text{He}$ ratio ($\sim 0.27R_a$), although helium alone could be used to trace an impactor
 342 (Mukhopadhyay et al., 2001).

343 It is extremely difficult to estimate the mass fraction of presolar nanodiamonds in the samples, as
 344 this deals with concentrations in the different endmembers, which are not well constrained.
 345 However, Huss et al. (Huss and Lewis, 1994) provide a typical concentration of ^{22}Ne of $\sim 8 \cdot 10^{-6}$
 346 $\text{cm}^3 \text{STP}\cdot\text{g}^{-1}$ for the carrier of Ne-A (pre-solar diamonds). If we assume a simple binary mixing
 347 between a terrestrial and extraterrestrial neon, we can calculate the mass fraction of
 348 extraterrestrial material in the NCF of sample 3404 as follow:

$$349 \quad \beta = \frac{R_{\text{measured}} - R_{\text{terrestrial}}}{R_{\text{diamonds}} - R_{\text{terrestrial}}} \sim 0.5 = \frac{C_{\text{diamonds}} M_{\text{diamonds}}}{C_{\text{measured}} M_{\text{measured}}} \sim \frac{8 \cdot 10^{-6} M_{\text{diamonds}}}{2 \cdot 10^{-10} M_{\text{measured}}}$$

350 Where R is the $^{20}\text{Ne}/^{22}\text{Ne}$ ratio. The term 0.5 is roughly estimated from Figure 3. We can
 351 therefore estimate a mass fraction of presolar diamonds carrying the neon-A signature in the
 352 NCF to be ~ 10 ppm. This however assumes that no neon loss has occurred and that the neon
 353 concentrations in nanodiamonds are well preserved during the impact and after. Using the
 354 $^3\text{He}/^{22}\text{Ne}$ of ~ 1 measured in presolar nanodiamonds, by Huss and Lewis (1994) we can also
 355 estimate the theoretical extraterrestrial ^3He within sample 3404. The calculation above suggests
 356 that half of the ^{22}Ne ($\sim 10^{-10} \text{ ccSTP/g}$) in the NCF should be of extraterrestrial origin and
 357 therefore the sample should contain $\sim 10^{-10} \text{ ccSTP/g}$ of extraterrestrial ^3He in the NCF. The NCF
 358 of sample 3404 contains only $\sim 5 \cdot 10^{-12} \text{ ccSTP/g}$ of total ^3He , much lower than expected from
 359 neon isotope calculation, suggesting either helium was lost during the impact or after deposition.

360

361

362 5.3.2 Evidence of an impact at the time sample 3404 m formed?

363

364 The presence of a Ne-A component would imply that an object impacted the Earth and that the
365 sedimentary rock at 3404 m would have included some ejecta containing the Ne-A component
366 during its formation. This could be related to the Acraman impact. The Acraman Lake in South
367 Australia is part of a deeply eroded impact structure in South Australia (Williams, 1986, 1994)
368 with an estimated original diameter of ~40-90 km (Haines, 2005), making it one of the ten
369 largest impact structures on Earth. The presence of ice-rafted material in layers directly below
370 and above the ejecta layer related to the Acraman impact structure, suggests that the Acraman
371 impact occurred during a phase of glaciation (Gostin et al., 2010). This could possibly
372 correspond to the Gaskiers glaciation dated at ~580 Ma (Bowring et al., 2003; Pu et al., 2016)
373 using U-Pb zircon geochronology on tuffs bracketing glacial diamictites. Similarly, (Walter et
374 al., 2000) suggested an age of 578 Ma for the Acraman impact using chemostratigraphic
375 correlation. However, the Acraman impact lacks a robust isotopic age for the ejecta layers due to
376 difficulties of dating (Schmieder et al., 2015). Thus, the age of the Acraman impact can only be
377 loosely constrained in the Ediacaran period between ~541 and ~635 Ma by stratigraphic
378 bracketing (Schmieder et al., 2015).

379 The layer at 3404 m, possibly containing the signature of Ne-A component, is not directly dated.
380 Nevertheless, the age range for the Nafun group layers has been assessed through correlations to
381 other sections (Fike et al., 2006) with U-Pb zircon ages obtained on ash beds (Bowring et al.,
382 2003; Pu et al., 2016). The unconformity below the 3836 m layer, at the base of the Shuram
383 formation, probably includes the time period of the ~580 Ma Gaskiers glaciation, based on
384 stratigraphic correlation (Bowring et al., 2003; Fike et al., 2006). The recovery of the Shuram
385 excursion (3300 m) is thought to have been completed by ~550 Ma (Condon et al., 2005). Thus,
386 the sample at 3404 m should have an age between ~580 and ~550 Ma (Figure 1). However, an
387 alternative view based on thermal subsidence curves to transform stratigraphic thicknesses of the
388 Nafun Group into time suggests that the basal Shuram is ~600 Myr (Le Guerroué et al., 2006). In
389 this scenario, the base on the Buah formation, where the layer at 3404 is located, might have an
390 age of ~575-570 Ma (Le Guerroué et al., 2006), close to the Acraman impact age of 578 Ma
391 determined by (Walter et al., 2000).

392 The estimated age range for the Acraman impact is thus consistent with the estimated time range
393 for the formation of the sample at 3404 m. Thus, the presence of an impact-derived Ne-A
394 component present in this sample that would witness an impact event is possible.

395

396 However, more precise age constraints for both the Acraman impact and for the deposition of the
397 Nafun group layers are required to confirm the validity of this hypothesis.

398

399

400 **6 Conclusion**

401

402 We have analyzed He and Ne isotopes in Ediacaran sedimentary rocks from the Nafun Group
403 strata, Sultanate of Oman that are believed to have been deposited between ~600-580 and ~550
404 Ma. Extraterrestrial He is still present in these samples and is in similar amounts to that found in
405 3 to 480 Myr old samples. However, we were unable to detect Ne isotopic composition of
406 interplanetary dust, unlike other data (Chavrit et al., 2016). This may be related to the higher
407 non-carbonate fraction in these samples as compared to previously published samples. Except for
408 one sample, the Ne isotopic composition follows a common nucleogenic trend, similar to those
409 defined by crustal fluids from the literature and the one predicted for the continental crust.
410 However, the other sample, from basal strata of the Buah formation, shows an unusual Ne
411 isotopic composition that can be explained by two hypotheses.

412 First, a singular nucleogenic trend deviating from the common nucleogenic trend could explain
413 the data. This would be the case if the sample contains a fluorine bearing mineral, such as
414 fluorite or fluorapatite, in amounts ranging respectively from 0.4 to 37% and 0.3 to 16% by
415 mass, depending on the U and Th contents of these minerals. Using SEM, we measured that the
416 sample contains ~0.15% fluorine and calcium rich phases. However, our estimates indicate that
417 this abundance is lower than the minimum fluorite proportion required to explain its singular Ne
418 composition. Nevertheless, our calculations are based on theoretical predictions and greatly rely
419 on the amount of U and Th used, which can lead to very different yields of ²⁰Ne produced after
420 600 Ma, and thus lead to a wide range for the required proportion of fluorine-bearing mineral
421 contained in this singular sample.

422 The other alternative is that this unusual Ne isotopic composition is related to the assimilation of
423 an extraterrestrial Ne-A component in this sample. This could be the result of a significant
424 meteoritic impact and, if so, would indicate that this highly volatile element was not lost to the
425 atmosphere upon the impact. This would be consistent with the Neoproterozoic Acraman impact

426 in Australia. However, the ages of both the impact event and the deposition of the basal Buah
427 Formation that contains the singular Ne isotopic composition are loosely constrained and more
428 precise ages are required to validate the impact hypothesis for the origin of the Ne signal
429 observed here.

430 For the time being, it is not possible to definitely rule out or validate one of the two hypotheses.
431 Future work will be to investigate the Ne isotopic composition of fluorine bearing minerals of
432 different ages to better assess their nucleogenic production over time. Sedimentary rocks
433 containing impact ejecta should also be analyzed.

434 Due to its signature in chondrites, Ne can potentially be an indicator of meteoritic impact in
435 sedimentary rocks. However, this study shows that in samples that are hundreds of million years
436 old, small amounts of F-bearing minerals can significantly affect the resulting Ne isotopic
437 composition. Thus, it is essential to consider the nucleogenic Ne production, in deciphering the
438 Ne isotopic composition in sedimentary rocks, especially for very old ones.

439

440

441 **Acknowledgments**

442

443 We thank the Oman Ministry of Oil and Gas for permission to publish this paper. We thank
444 Stephan Borensztajn for assistance during with the SEM measurements and Cécile Gautheron for
445 providing the Durango fluorapatite. FM thanks the European Research Council under the
446 European Community's H2020 framework program/ERC grant agreement # 637503 (Pristine),
447 the Agence Nationale de la Recherche for a chaire d'Excellence Sorbonne Paris Cité
448 (IDEX13C445) and the Plateform PARI. FM and MM thank the UnivEarthS Labex program
449 (ANR-10-LABX-0023 and ANR-11-IDEX-0005-02). P. Sarda, J. Hopp and the two other
450 anonymous reviewers are thanked for their constructive reviews. This is IGP contribution
451 number 4027.

452

453

454 **References**

455

- 456 Alvarez , L.W., Alvarez, W., Asaro , F. and Michel , H.V. (1980) Extraterrestrial cause for the
457 Cretaceous-Tertiary extinction. *Science* 208, 1095.
- 458 Amari, S. and Ozima, M. (1988) Extra-terrestrial noble gases in deep-sea sediments. *Geochimica*
459 *et Cosmochimica Acta* 52, 1087-1095.
- 460 Ballentine, C.J. and Burnard, P.G. (2002) Production, Release and Transport of Noble Gases in
461 the Continental Crust. *Rev. Mineral. Geochem* 47, 481-538.
- 462 Black, D.C. (1972) On the origins of trapped helium, neon and argon isotopic variations in
463 meteorites—I. Gas-rich meteorites, lunar soil and breccia *Geochimica et Cosmochimica*
464 *Acta* 36, 347-375.
- 465 Bowring , S., Myrow, P., Landing, E., Ramezani , J. and Grotzinger, J. (2003) Geochronological
466 constraints on terminal Neoproterozoic events and the rise of Metazoan. EGS - AGU -
467 EUG Joint Assembly, Abstracts from the meeting held in Nice, France, 6 - 11 April 2003
468 abstract #13219.
- 469 Burns, S.J. and Matter, A. (1993) Carbon isotopic record of the latest Proterozoic from Oman.
470 *Eclogae Geologicae Helveticae* 86, 595-607.
- 471 Chavrit, D., Moreira, M. and Moynier , F. (2016) Estimation of the extraterrestrial ^3He and ^{20}Ne
472 fluxes on Earth from He and Ne systematics in marine sediments. *Earth and Planetary*
473 *Science Letters* 436, 10-18.
- 474 Clarke, W.B., Jenkins, W.J. and Top, Z. (1976a) Determination of tritium by mass spectrometric
475 measurement of ^3He . *The International Journal of Applied Radiation and Isotopes* 27, 512-
476 522.
- 477 Clarke, W.B., Jenkins, W.J. and Top, Z. (1976b) Determination of tritium by mass spectrometric
478 measurement of ^3He . *Int. J. Appl. radiat. Isot.* 27, 515-522.
- 479 Condon, D., Zhu , M., Bowring, S., Wang, W., Yang , A. and Jin , Y. (2005) U-Pb Ages from the
480 Neoproterozoic Doushantuo Formation, China. *Science* 308, 95.
- 481 Darrah, T.H. and Poreda, R. (2012) Evaluating the accretion of meteoritic debris and
482 interplanetary dust particles in the GPC-3 sediment core using noble gas and mineralogical
483 tracers. *Geochim. Cosmoch. Acta* 84, 329-352.
- 484 Drescher, J., Kirsten, T. and Schafer, K. (1998) The rare gas inventory of the continental crust,
485 recovered by the KTB continental deep drilling project. *Earth and Planetary Science*
486 *Letters* 154, 247-263.

487 Eberhardt, P., Eugster, E. and Marti, K. (1965) A redetermination of the isotopic composition of
488 atmospheric neon. *Z. Naturforsch.* 20a, 623-624.

489 Eikenberg, J., Signer, P. and Wieler, R. (1993) U-Xe, U-Kr, and U-Pb systematics for dating
490 uranium minerals and investigations of the production of nucleogenic neon and argon.
491 *Geochim. Cosmoch. Acta* 57, 1053-1069.

492 Farley, K.A., Shoemaker, E.M., Montanari, A. and Patterson, D.B. (1997) Helium-3 evidence for
493 a comet shower in the late Eocene. Seventh annual V. M. Goldschmidt conference,
494 Tucson, AZ, United States, June 2-6, 1997 LPI Contribution, vol.921, pp.68-69, 1997.

495 Farley, K.A., Vokrouhlicky, D., Bottke, W.F. and Nesvorny, D. (2006) A late Miocene dust
496 shower from the break-up of an asteroid in the main belt. *Nature* 439, 295-297.

497 Fike, D.A., Grotzinger, J.P., Pratt, L.M. and Summons, R.E. (2006) Oxidation of the Ediacaran
498 Ocean. *Nature* 444, 744-747.

499 Gautheron, C., tassin-Got, L. and Farley, K.A. (2006) (U-Th)/Ne chronometry. *Earth and*
500 *Planetary Science Letters* 243, 520-535.

501 Gostin, V.A., McKirdy, D.M., Webster, L.J. and Williams, G.E. (2010) Ediacaran ice-rafting and
502 coeval asteroid impact, South Australia: insights into the terminal Proterozoic
503 environment. *Australian Journal of Earth Sciences* 57, 859-869.

504 Grotzinger, J.P., Bowring, S.A., Saylor, B.Z. and Kaufman, A.J. (1995) Biostratigraphic and
505 geochronologic constraints on early animal evolution. *Science* 270, 598.

506 Grotzinger, J.P., Fike, D.A. and Fischer, W.W. (2011) Enigmatic origin of the largest-known
507 carbon isotope excursion in Earth's history. *Nature Geosci* 4, 285-292.

508 Haines, P.W. (2005) Impact cratering and distal ejecta: the Australian record. *Australian Journal*
509 *of Earth Sciences* 52.

510 Hildebrand, A.R., Penfield, G.T., Kring, D.A., Pilkington, M., Camargo Z., A., Jacobsen, S.B.
511 and Boynton, W.V. (1991) Chicxulub Crater: a possible Cretaceous/Tertiary boundary
512 impact crater on the Yucatán Peninsula, Mexico. *Geology* 19, 867-871.

513 Hiyagon, H. (1994) Retention of Solar Helium and Neon in IDPs in Deep Sea Sediment. *Science*
514 263, 1257-1259.

515 Holland, G., Sherwood Lollar, B., Li, L., Lacrampe-Couloume, G., Slater, G.F. and Ballentine,
516 C.J. (2013) Deep fracture fluids isolated in the crust since the Precambrian era. *Nature* 497,
517 357-360.

- 518 Hünemohr, H. (1989) Edelgase in U- und Th-reichen Mineralen und die Bestimmung der ^{21}Ne -
519 Dicktarget-Ausbeute der $^{18}\text{O}(\text{a},\text{n})^{21}\text{Ne}$ -Kernreaktion im Bereich 4.0 - 8.8 MeV. Johannes-
520 Gutenberg-Universität in Mainz.
- 521 Huss, G.R. and Lewis, R. (1994) Noble gases in presolar diamonds II : Component abundances
522 reflect thermal processing. *Meteoritics* 29, 811-829.
- 523 Kennedy, B.M., Hiyagon, H. and Reynolds, J.H. (1990) Crustal neon: a striking uniformity.
524 *Earth and Planetary Science Letters* 98, 277-286.
- 525 Le Guerroué, E. (2010) Duration and synchronicity of the largest negative carbon isotope
526 excursion on Earth: The Shuram/Wonoka anomaly. *Comptes Rendus Geoscience* 342, 204-
527 214.
- 528 Le Guerroué, E., Allen, P.A., Cozzi, A., Etienne, J.L. and Fanning, M. (2006) 50 Myr recovery
529 from the largest negative $\delta^{13}\text{C}$ excursion in the Ediacaran ocean. *Terra Nova* 18, 147-153.
- 530 Le Guerroué, E. and Cozzi, A. (2010) Veracity of Neoproterozoic negative C-isotope values: the
531 termination of the Shuram negative excursion. *Gondwana Research* 17, 653-661.
- 532 Lippmann-Pipke, J., Sherwood Lollar, B., Niedermann, S., Stroncik, N.A., Naumann, R., van
533 Heerden, E. and Onstott, T.C. (2011) Neon identifies two billion year old fluid
534 component in Kaapvaal Craton. *Chem. Geol.* 283, 287-296.
- 535 Marcantonio, F., Kumar, N., Stute, M., Anderson, R.F., Seidl, M.A., Schlosser, P. and Mix, A.
536 (1995) A comparative study of accumulation rates derived by He and Th isotope analysis
537 of marine sediments. *Earth and Planetary Science Letters* 133, 549-555.
- 538 McGee, D. and Mukhopadhyay, S. (2013) Extraterrestrial He in sediments: from recorder of
539 asteroid collisions to timekeeper of global environmental change. in: Burnard, P.G. (Ed.),
540 *The Noble Gases as Geochemical Tracers*. Springer Berlin Heidelberg, 155-176.
- 541 Moreira, M. (2013) Noble gas constraints on the origin and evolution of earth's volatiles.
542 *Geochemical Perspectives* 2, 229-403.
- 543 Moreira, M. and Allègre, C.J. (2002) Rare gas systematics on Mid Atlantic Ridge (37°-40°).
544 *Earth and Planetary Science Letters* 198, 401-416.
- 545 Moreira, M. and Charnoz, S. (2016) Origin of the neon in Earth and in chondrites. *Earth and*
546 *Planetary Science Letters* 433, 249-256.

547 Mougél , B., Moynier, F., Göpel, C. and Koeberl , C. (2017) Chromium isotope evidence in
548 ejecta deposits for the nature of Paleoproterozoic impactors. *Earth and Planetary Science*
549 *Letters* 460, 105-111.

550 Mukhopadhyay, S., Farley, K.A. and Montanari, A. (2001) A short duration of the Cretaceous-
551 Tertiary boundary event: evidence from extraterrestrial Helium-3. *Science* 291, 1952-1955.

552 Murphy, B.H., Farley , K.A. and Zachos, J.C. (2010) An extraterrestrial ^3He -based timescale for
553 the Paleocene–Eocene thermal maximum (PETM) from Walvis Ridge, IODP Site 1266.
554 *Geochim. Cosmoch. Acta* 74, 5098-5108.

555 Patterson, D.B., Farley, K.A. and Schmitz, B. (1998) Preservation of extraterrestrial ^3He in 480-
556 Ma-old marine limestones. *Earth and Planetary Science Letters* 163, 315-325.

557 Pepin, R.O. (1967) Trapped neon in meteorites. *Earth and Planetary Science Letters* 2, 13-18.

558 Peucker-Ehrenbrink , B. (2001) Iridium and osmium as tracers of extraterrestrial matter in
559 marine sediments. in: Peucker-Ehrenbrink, B., Schmitz, B. (Eds.), *Accretion of*
560 *extraterrestrial matter throughout Earth's history*. Springer Science+Business Media, New
561 York, 163-178.

562 Pu, J.P., Bowring, S.A., Ramezani, J., Myrow, P., Raub, T.D., Landing, E., Mills, A., Hodgin, E.
563 and Macdonald, F.A. (2016) Dodging snowballs: geochronology of the Gaskiers glaciation
564 and the first appearance of the Ediacaran biota. *Geology*.

565 Schmieder, M., Tohver, E., Jourdan, F., Denyszyn, S.W. and Haines, P.W. (2015) Zircons from
566 the Acraman impact melt rock (South Australia): shock metamorphism, U–Pb and
567 $^{40}\text{Ar}/^{39}\text{Ar}$ systematics, and implications for the isotopic dating of impact events.
568 *Geochimica et Cosmochimica Acta* 161, 71-100.

569 Sharpton, V.L., Brent Dalrymple, G., Marin, L.E., Ryder, G., Schuraytz, B.C. and Urrutia-
570 Fucugauchi, J. (1992) New links between the Chicxulub impact structure and the
571 Cretaceous/Tertiary boundary. *Nature* 359, 819-821.

572 Takayanagi, M. and Ozima, M. (1987) Temporal variation of $^3\text{He}/^4\text{He}$ ratio recorded in deep-sea
573 sediment cores. *Journal of Geophysical Research* 92, 12531-12538.

574 Walter, M.R., Veevers , J.J., Calver , C.R., Gorjan, P. and Hill, A.C. (2000) Dating the 840–544
575 Ma Neoproterozoic interval by isotopes of strontium, carbon, and sulfur in seawater, and
576 some interpretative models. *Precambrian Res.* 100, 371-433.

577 Williams, G.E. (1986) The Acraman impact structure: source of ejecta in late Precambrian
578 shales, South Australia. *Science* 233, 200--203.

579 Williams, G.E. (1994) Acraman, South Australia: Australia's largest meteorite impact structure.
580 *Proc. Royal Soc. Victoria* 106.

581 Yatsevich, I. and Honda, M. (1997) Production of nucleogenic neon in the Earth from natural
582 radioactive decay. *Journal of Geophysical Research* 102, 10291-10298.

583

584

Figure Captions

585

586

587 **Figure 1:** The noble gas composition as a function of depth. NCF = non-carbonate fraction.
588 Error bars for the isotopic ratios are smaller than or equal to the symbol size when non visible.
589 The $\delta^{13}\text{C}$ carbonates data are from (Fike et al., 2006). Geochronological constraints are from
590 (Bowring et al., 2003; Condon et al., 2005; Fike et al., 2006 ; Grotzinger et al., 1995; Le
591 Guerroué et al., 2006). The Khufai and Shuram formations are separated by an unconformity
592 (wavy curve) that probably includes the Gaskiers glaciation (Bowring et al., 2003). The dotted
593 lines are the limits of the Shuram carbon isotope negative excursion (Fike et al., 2006).

594

595 **Figure 2:** $^3\text{He}/^4\text{He}$ ratio versus ^3He contents. The lines represent mixing lines between an IDP
596 component, rich in ^3He , with $^3\text{He}/^4\text{He}=2.4\times 10^{-4}$ and two hypothetical terrestrial endmembers,
597 rich in radiogenic ^4He and poor in ^3He considering $^3\text{He}/^4\text{He}=10^{-9}$ - 10^{-7} . The 2 mixing lines are
598 derived from (McGee and Mukhopadhyay, 2013). Examples of literature data (small grey dots)
599 are from (Chavrit et al., 2016; Farley et al., 2006; Murphy et al., 2010) , and Chavrit et al.
600 (unpublished data).

601

602

603 **Figure 3:** $^{20}\text{Ne}/^{22}\text{Ne}$ ratios versus $^{21}\text{Ne}/^{22}\text{Ne}$ ratios. Sedim. stands for sediments or sedimentary
604 rocks, mfl = mass fractionation line. The plain lines are nucleogenic trends for different O/F
605 ratios (atomic ratios). Cont. crust (=continental crust predicted) is from (Yatsevich and Honda,
606 1997). The measured crustal fluids trend with a O/F=113 (Ballentine and Burnard, 2002) is
607 obtained from the nucleogenic trend defined by the crustal fluid data from (Kennedy et al.,
608 1990). The line “KTB” represents the continental crust as sampled by the KTB drill in Germany
609 (Drescher et al., 1998). The slopes of the mixing lines between the air component and the
610 nucleogenic components are a function of the O/F ratio (presented as atomic ratios here). The
611 compositions of IDP are close to that of the Ne-B value ($^{20}\text{Ne}/^{22}\text{Ne}=12.73\pm 0.02$,
612 $^{21}\text{Ne}/^{22}\text{Ne}=0.0321\pm 0.0001$) (Moreira, 2013), the Ne-A composition is from (Huss and Lewis,
613 1994), the air composition is from (Eberhardt et al., 1965).

614

615 **Figure 4:** Slope of the line passing through the air component and a given sample (reflecting the
616 O/F value) in the three Ne isotopes diagram (Figure 3) as a function of the depth. The unusual
617 Ne composition characterizes a negative spike at the depth 3404 m. The dotted lines indicate the
618 limits of the Shuram excursion (Figure 1).

619

620

621 **Figure 5 :** Nuclear reactions producing Ne isotopes in the crust.

622

623

624 **Figure 6:** SEM-EDS mapping of the residual powders (=non-carbonate fractions, NCF) of
625 several samples from this study. All the acquisitions were done with a resolution of 467 nm.px⁻¹.

626

627

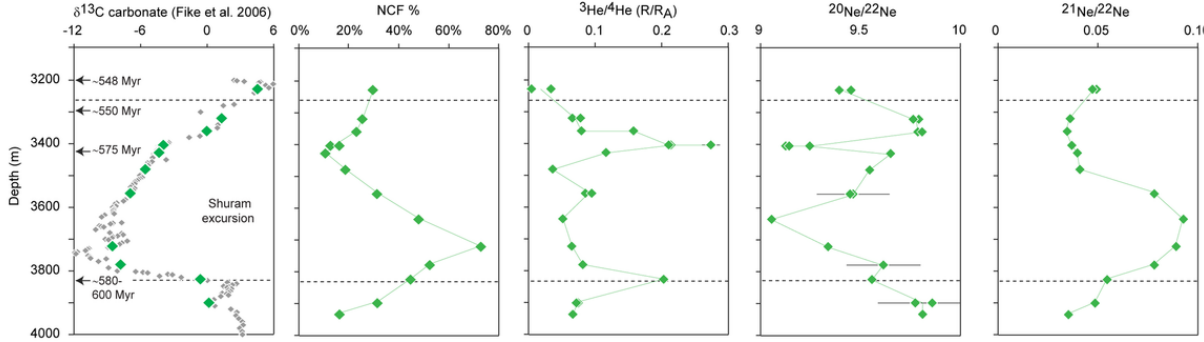
628 Table 1: Helium and Ne concentrations and isotopic composition of the sedimentary rocks from
629 the Huqf Supergroup and fluorapatites analyzed in this study using the Noblesse mass
630 spectrometer sited at IPGP. Durango fluorapatites were analyzed in 2006 using the ARESIBO
631 mass spectrometer sited at that time in IPGP. Helium and neon concentrations for these three
632 samples cannot be compared to other Durango analyses since these samples were baked under
633 vacuum before analysis.

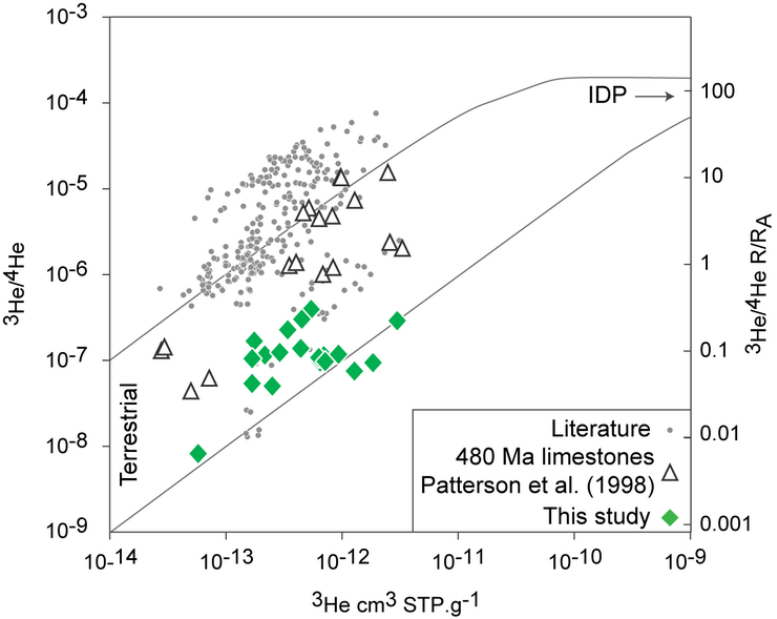
634 The sample units, depths and lithologies are from (Fike et al., 2006). In the text, the samples
635 names used correspond to their depth of collection in the drill hole (2nd column of this table).
636 Dup. = duplicate. NCF=non-carbonate fractions, corresponding to residual weight/initial weight
637 ratio in percent. *For the sedimentary rocks, the loaded mass is estimated from the residual
638 fraction after leaching. R_A is the atmospheric $^3\text{He}/^4\text{He}$ ratio (1.384×10^{-6} ; (Clarke et al., 1976a).
639 The concentrations are expressed in $\text{cm}^3 \text{STP.g}^{-1}$ of initial mass. Uncertainties are $\pm 5\%$ on
640 absolute abundances and $\pm 2\%$ on element ratios. #indicates the sample with the unusual Ne
641 composition.

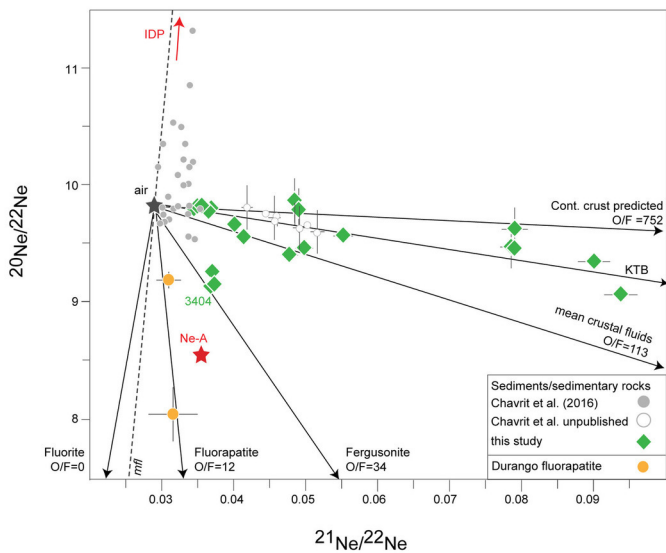
642

Sample unit	Sample depth (m)	Sample lithology	Dup. #	Loaded mass* g	NC F %	⁴ He ×10 ⁻⁶	³ He/ ⁴ He ×10 ⁻⁷	σ	³ He/ ⁴ He R/R _A	σ	²² Ne ×10 ⁻¹¹	²⁰ Ne/ ²² Ne	σ	²¹ Ne/ ²² Ne	σ
Sedimentary rocks															
Buah	3228	silty dolostone	1	0.1567	30%	7.43	0.08	0.04	0.006	±0.003	5.31	9.45	±0.03	0.0497	±0.0012
			2	0.1428	30%	5.33	0.48	0.05	0.035	±0.004	5.51	9.39	±0.03	0.0477	±0.0012
Buah	3320	silty dolostone	1	0.1449	25%	7.22	0.92	0.07	0.067	±0.005	8.77	9.79	±0.03	0.0369	±0.0007
			2	0.0891	25%	6.57	1.09	0.08	0.079	±0.006	8.10	9.76	±0.03	0.0365	±0.0007
Buah	3360	dolostone	1	0.1135	23%	1.59	2.19	0.14	0.158	±0.010	5.59	9.79	±0.03	0.0345	±0.0009
			2	0.0987	23%	1.99	1.11	0.14	0.081	±0.010	6.64	9.81	±0.03	0.0350	±0.0009
Buah	3404#	dolostone	1	0.1092	13%	1.58	2.97	0.16	0.214	±0.011	2.35	9.25	±0.03	0.0370	±0.0008
			2	0.1409	16%	1.46	3.79	0.19	0.274	±0.013	2.37	9.13	±0.03	0.0368	±0.0009
			3	0.1905	16%	1.59	2.92	0.13	0.211	±0.009	2.32	9.14	±0.03	0.0373	±0.0009
Buah	3428	dolostone	1	0.0623	11%	1.11	1.62	0.07	0.117	±0.005	2.11	9.65	±0.03	0.0401	±0.0010
Shuram	3480	silty limestone	1	0.1514	19%	3.31	0.52	0.15	0.037	±0.011	5.00	9.55	±0.03	0.0414	±0.0008
Shuram	3556	silty limestone	1	0.1556	31%	2.49	1.20	0.02	0.086	±0.002	5.04	9.34	±0.07	0.0777	±0.0013
			2	0.1892	31%	3.40	1.33	0.03	0.096	±0.002	4.81	9.45	±0.03	0.0788	±0.0005
Shuram	3636	silty limestone	1	0.1534	48%	18.13	0.73	0.12	0.052	±0.009	8.13	9.05	±0.03	0.0935	±0.0023
Shuram	3722	calcareous shale	1	0.1543	73%	21.02	0.91	0.07	0.066	±0.005	10.42	9.34	±0.03	0.0898	±0.0022
Shuram	3780	silty limestone	1	0.1031	52%	8.41	1.14	0.02	0.082	±0.001	6.79	9.49	±0.07	0.0782	±0.0016
Shuram	3826	limestone/sandstone	1	0.1476	45%	10.98	2.82	0.07	0.204	±0.005	7.76	9.56	±0.03	0.0551	±0.0014
Khufai	3900	dolostone	1	0.1297	31%	6.19	1.05	0.02	0.076	±0.002	8.71	9.73	±0.07	0.0480	±0.0008
			2	0.1956	31%	1.70	1.01	0.02	0.073	±0.002	2.75	9.65	±0.07	0.0486	±0.0008
Khufai	3936	limestone	1	0.1544	16%	7.89	0.93	0.05	0.067	±0.004	14.69	9.81	±0.01	0.0356	±0.0001
Durango fluorapatite															
DUR3-1				0.012		120					25.20	9.19	±0.07	0.0310	±0.0017
DUR4-2				0.010		100					2.88	8.05	±0.23	0.0316	±0.0034
DUR5-3				0.014		150					2.59	2.90	±0.30	0.0349	±0.0035

formation



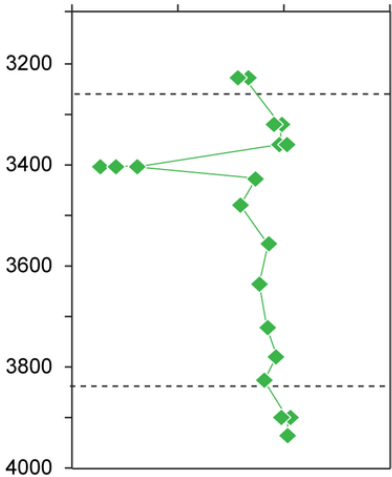


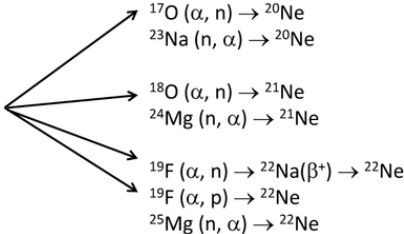
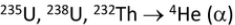


slope of mixing line in Ne diagram

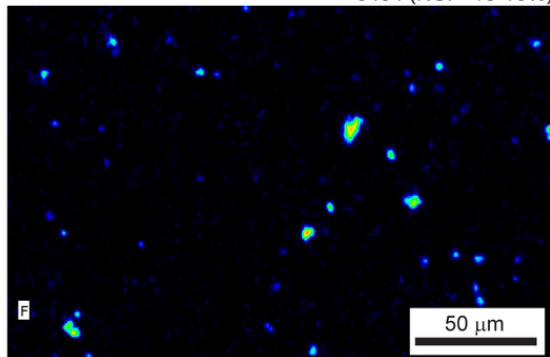
-100 -50 0 50

Depth (m)

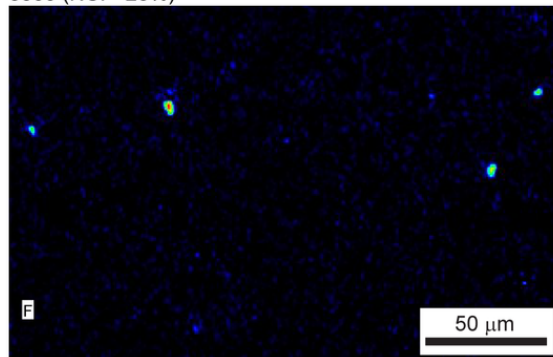




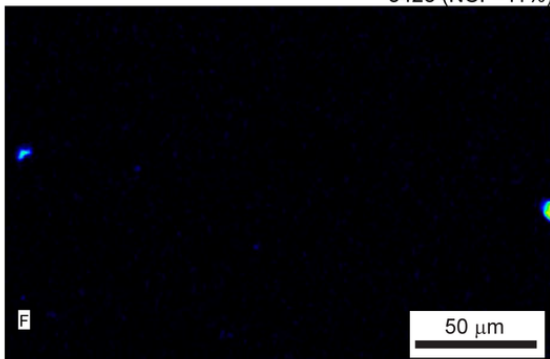
3404 (NCF=13-16%)



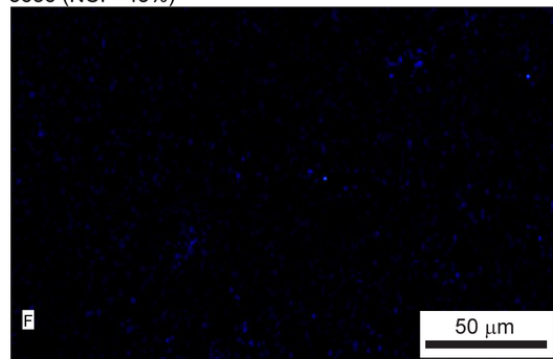
3360 (NCF=23%)



3428 (NCF=11%)



3636 (NCF=48%)



3228 (NCF=30%)

